



Research article

Prediction of small intracranial aneurysm rupture status based on combined Clinical–Radiomics model

Yu Ye^{a,1}, Jiao Chen^{a,1}, Xiaoming Qiu^a, Jun Chen^b, Xianfang Ming^a, Zhen Wang^a, Xin Zhou^{a,**}, Lei Song^{a,*}

^a Department of Radiology, Huangshi Central Hospital, Affiliated Hospital of Hubei Polytechnic University, Huangshi, China

^b GE Health Care, Wuhan, China

ABSTRACT

Background: Accumulating small unruptured intracranial aneurysms are detected due to the improved quality and higher frequency of cranial imaging, but treatment remains controversial. While surgery or endovascular treatment is effective for small aneurysms with a high risk of rupture, such interventions are unnecessary for aneurysms with a low risk of rupture. Consequently, it is imperative to accurately identify small aneurysms with a low risk of rupture. The purpose of this study was to develop a clinically practical model to predict small aneurysm ruptures based on a radiomics signature and clinical risk factors.

Methods: A total of 293 patients having an aneurysm with a diameter of less than 5 mm, including 199 patients (67.9 %) with a ruptured aneurysm and 94 patients (32.1 %) without a ruptured aneurysm, were included in this study. Digital subtraction angiography or surgical treatment was required in all cases. Data on the clinical risk factors and the features on computed tomography angiography images associated with the aneurysm rupture status were collected simultaneously. We developed a clinical–radiomics model to predict aneurysm rupture status using multivariate logistic regression analysis. The combined clinical–radiomics model was constructed by nomogram analysis. The diagnostic performance, clinical utility, and model calibration were evaluated by operating characteristic curve analysis, decision curve analysis, and calibration analysis.

Results: A combined clinical–radiomics model (Area Under Curve [AUC], 0.85; 95 % confidence interval [CI], 0.757–0.947) showed effective performance in the operating characteristic curve analysis. In the validation cohort, the performance of the combined model was better than that of the radiomics model (AUC, 0.75; 95 % CI, 0.645–0.865; Delong's test p-value = 0.01) and the clinical model (AUC, 0.74; 95 % CI, 0.625–0.851; Delong's test p-value <0.01) alone. The results of the decision curve, nomogram, and calibration analyses demonstrated the clinical utility and good fitness of the combined model.

Conclusion: Our study demonstrated the effectiveness of a clinical–radiomics model for predicting rupture status in small aneurysms.

1. Introduction

Intracranial aneurysm refers to the localized and pathological dilation of intracranial artery walls, leading to a risk of rupture. Aneurysm rupture is the main cause of spontaneous subarachnoid hemorrhage [1]. Aneurysmal subarachnoid hemorrhage is a cerebrovascular disease that seriously endangers human health due to its large number, wide range, and poor prognosis. The overall incidence of intracranial aneurysms in adults worldwide is 3.2 % [2]. Nearly 50 % of the detected intracranial aneurysms are less than

* Corresponding author. Department of Radiology, Huangshi Central Hospital, Affiliated Hospital of Hubei Polytechnic University, No. 141, Tianjin Road, Huangshigang District, Huangshi 435000, China.

** Corresponding author. Department of Radiology, Huangshi Central Hospital, Affiliated Hospital of Hubei Polytechnic University, No. 141, Tianjin Road, Huangshigang District, Huangshi 435000, China.

E-mail addresses: 819137808@qq.com (X. Zhou), song580lei@163.com (L. Song).

¹ These authors contributed equally.

<https://doi.org/10.1016/j.heliyon.2024.e30214>

Received 24 November 2023; Received in revised form 21 April 2024; Accepted 22 April 2024

Available online 24 April 2024

2405-8440/© 2024 Published by Elsevier Ltd.

This is an open access article under the CC BY-NC-ND license

(<http://creativecommons.org/licenses/by-nc-nd/4.0/>).

5 mm in diameter [3]. Some studies identified aneurysm size as the most critical factor to predict aneurysm stability [4], with a low probability of enlargement for small aneurysms [5,6]. Greving et al. [7] also showed that the risk of rupture was much lower than the risk of surgical complications for many small intracranial aneurysms. However, Lai et al. [8] showed that 64 % of ruptured aneurysms were small aneurysms. Meanwhile, another study also showed that ruptured small intracranial aneurysms was a common cause of aneurysmal subarachnoid hemorrhage, who should be actively managed [9]. However, the treatment of patients with unruptured small aneurysms (diameter <5 mm) has been controversial, and there are no unified standard recommendations. Therefore, predicting the risk of small aneurysm rupture is crucial for determining patient prognosis and designing personalized treatment strategies.

Researchers recommend the use of various rupture risk factors (such as clinical and epidemiological factors) [7,10–13] for constructing scoring systems. To date, PHASES (based on population, hypertension, age, size of aneurysm, earlier subarachnoid hemorrhage, and site) is the scoring system most commonly applied in the clinic. However, the research methods and data sources used for designing PHASES have limited its wider application [12]. Morphology has also been identified as a biomarker of aneurysm status in previous studies. However, these morphological parameters were only measured in a two-dimensional projection and measurement variability may be introduced by different readers, raters, and projections, which may undermine the comparability of results [14–16]. Small aneurysms, in particular, must be specifically modeled due to their unique histological features. Therefore, new methods are needed to model the rupture risk of small aneurysms to facilitate clinical decision-making.

Radiomics can be used to extract a large number of quantitative features from medical images to construct a prediction model for disease through high-throughput analysis and feature selection [17]. Previous studies have confirmed that the radiomics features extracted from the computed tomography angiography (CTA) images of aneurysms can be used to evaluate their rupture risk [18]. Several studies have focused on establishing radiomics diagnostic models to predict intracranial aneurysm rupture [18–20]. However, few studies have attempted to predict the rupture risk of aneurysms with a diameter <5 mm. Therefore, we propose to use CTA radiomics data in conjunction with clinical factors to develop and validate a clinically practical nomogram to predict the rupture status of small intracranial aneurysms (<5 mm).

2. Materials and methods

2.1. Study population

The inclusion criteria for this study were all patients who underwent CTA examination from January 2018 to March 2021. Aneurysms were confirmed by Digital subtraction angiography (DSA) or surgery, and the time interval between CTA and DSA or surgery was not longer than one month (n = 632). The exclusion criteria were the following: (1) no aneurysms (n = 395); (2) patients with arteriovenous malformation (n = 20), Moyamoya disease (n = 43), or incomplete image/clinical aneurysms data (n = 24); (3) patients

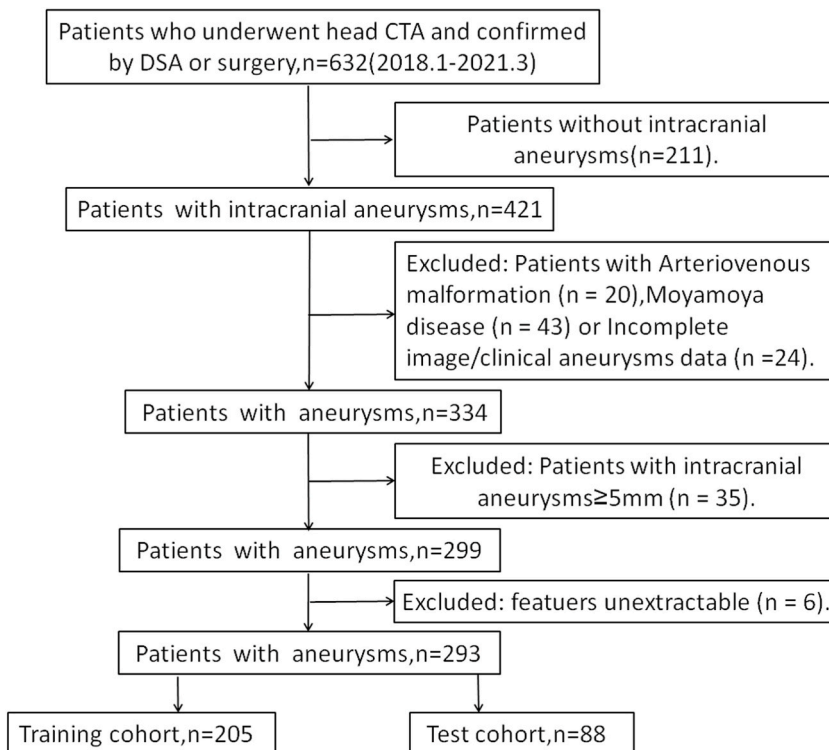


Fig. 1. Flowchart of patient inclusion and exclusion process.

with intracranial aneurysms ≥ 5 mm ($n = 35$); and (4) features unextractable ($n = 6$). Finally, a total of 293 aneurysms with diameter < 5 mm were included. The aneurysm data were randomly divided into training cohorts ($n = 206$) and test cohorts ($n = 88$) in a ratio of 7:3. This study was a retrospective study, which was approved by the Huangshi Central Hospital. The patient's right to informed consent was waived.

The flowchart in Fig. 1 illustrates the process of inclusion and exclusion of patients. The study workflow is shown in Fig. 2.

2.2. Clinical and imaging data

The clinical data was collected from the patients' hospitalization history. Basic clinical information included gender and age. Medical history included smoking, drinking, hypertension, diabetes, heart disease, thyroid disease, stroke, cancer, aspirin use, uric acid abnormality, hyperlipidemia, family history. CTA imaging findings included the number, size, and location of intracranial aneurysms (including internal carotid artery, anterior cerebral artery, middle cerebral artery, posterior cerebral artery, anterior communicating artery, vertebral artery, basilar artery, and anterior choroidal artery) [7,10–13]. The patients were divided into the ruptured aneurysm group and the unruptured aneurysm group as follows: 1) When SAH patients had only one aneurysm found by CTA and it was consistent with the bleeding location, it was identified as a ruptured aneurysm; 2) When CTA found one aneurysm and it was inconsistent with the bleeding location, DSA was used for identifying the rupture state; 3) When CTA found two or more aneurysms, the ruptured state of the respective aneurysms was confirmed intraoperatively [21]. Among all the participants, 94 cases had no clinical symptoms. The aneurysms were found due to physical examination or other ruptured intracranial aneurysms, and were thus defined as unruptured aneurysms.

2.3. Imaging techniques

GE (Light Speed) 64-slice CT was used to collect raw imaging data. The patient was in the supine position. The scanning baseline was set to be parallel to the auditory canthal line and the scanning range was from the base of the skull to the top of the skull. The scanning parameters were the following: tube voltage, 120 kV; tube current, 350 mA; and pitch, 1; layer thickness, 0.625. The contrast agent was iodixanol containing 320 mg/ml iodine (US General Pharmaceutical Industry), which was injected with normal saline using an automatic double-barrel high-pressure syringe (MADRAD, US). The contrast agent injection dose (mL) was calculated as the body weight (kg) \times 0.9 (ml/kg), and the injection flow rate was 4.5 ml/s. After the contrast agent was injected, 40 ml of normal saline was injected at a flow rate of 4.5 ml/s.

2.4. Image segmentation, pre-processing, and feature extraction

Two radiologists with 7 and 10 years of experience in the imaging diagnosis of the central nervous system independently used the blind method (without knowing the patient's clinical information and aneurysm rupture status) to manually delineate the region of interest around the intracranial aneurysms in three directions with 3D slicer 4.10.1 (<https://www.slicer.org/>), using a window width

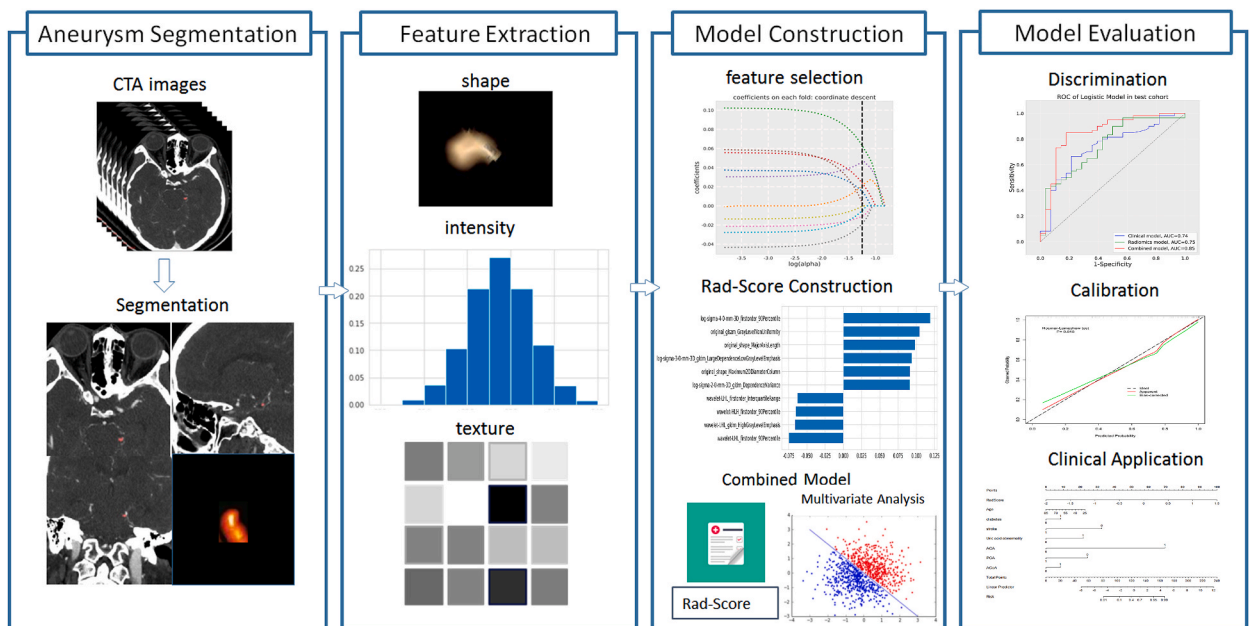


Fig. 2. Study flowchart.

of 800 and a window level of 240. Then, the two radiologists visually compared the sketching results. If there were differences, the final sketching results of the region of interest were obtained after discussion.

2.5. Feature extraction

First, the CT images were resampled using a spline interpolation algorithm to ensure radiographic consistency between images acquired from different scanners. Second, we extracted radiomics features from the data with the PyRadiomics software (<https://pyradiomics.readthedocs.io/>). For each patient, 1211 radiomics features were extracted from the CTA images. There were seven different radiomics features: shape features; first order features; gray level co-occurrence matrix (GLCM) features; gray level dependence matrix (GLDM) features; gray level run length matrix (GLRLM) features; gray level size zone matrix (GLSZM) features; and neighborhood gray-tone difference matrix (NGTDM) features. The quantitative radiomics features were derived from three types of images: the original image, the Laplacian of Gaussian (LoG) image, and the wavelet image, which was obtained through eight decompositions after wavelet filtering. In three dimensions, applying a high- or low-pass filter yielded eight combinations. The LoG image was generated using a LoG filter along with a sequence of sigma values. During this study, the sigma values 2, 3, and 4 were used, respectively.

2.6. Feature selection, and development and validation of radiomics signature

The dimensionality of radiomics features was reduced in three steps. The first step involved selecting radiomics features with a variance greater than 1.0. Next, the analysis of variance (ANOVA) method was used to determine the statistical influence feature for rupture status in intracranial aneurysms. Last, radiomics features were retrieved from the training cohort by using the least absolute shrinkage and selection operation (LASSO) regression method, which was used to select features associated with the classification that had non-zero coefficients. In the LASSO regression, the radiomics score (rad score) was computed using an algorithm that combined the selected features and weighted them by their coefficients. The radiomics signature development and feature selection were both carried out in the training cohort. Accordingly, the performance of the obtained radiomics signature was evaluated using an inter-validation cohort, which was not used for the model development.

2.7. Clinical and combined models

We extracted the clinical features from the training cohort that were proven significant by chi-squared tests (categorical variables) or Student's t-tests and Wilcoxon tests (continuous variables). Subsequent investigation was undertaken using backward stepwise multivariate logistic analysis to find a discriminative clinical feature and build a clinical and radiology (CR) model.

2.8. Model construction, calibration, and validation

Patients were randomly assigned to a training and validation cohorts in a ratio of 7:3. Within the training cohort, three models were established: (1) a radiomics model (based on rad-scores); (2) a clinical model (based on clinical factors); and (3) a hybrid model (based on clinical–radiomics scores). Analysis of discrimination ability, model calibration, and clinical utility all confirmed the models' diagnostic performance and their fitness as diagnostic models.

2.9. Discrimination ability

We evaluated the discrimination ability of the rupture status models by using receiver operating curves (ROCs). The discrimination performance is presented via bar charts. Furthermore, the constructed models were evaluated for accuracy, precision, sensitivity, and specificity.

2.10. Model calibration

Both the training test and independent validation cohorts were calibrated to determine whether the observed outcome and the predicted probabilities agreed. A p -value greater than 0.05 was considered to indicate a well-calibrated model using the Hosmer-Lemeshow test.

2.11. Clinical utility

A decision curve analysis was used to evaluate the clinical utility of the built models at different threshold probabilities in the three cohorts. Multivariable logistic regression was used to formulate a nomogram based on radiomics and clinical factors.

2.12. Statistical analysis

R software (version 4.1.1) and Python 3.7 (version 3.7) were used to conduct all statistical analyses. The clinical factors were analyzed using the Chi-square test, independent-samples t -test, or Mann-Whitney U test according to the distribution of variables with

scipy (version 1.7.0). The Shapiro-Wilk test was used to test for normality. To compare the AUC values of the three models, we performed Delong’s non-parametric test. To assess the fitness of the three models, the Hosmer-Lemeshow test was used. Statistical significance was defined as $p < 0.05$ in all analyses.

3. Results

3.1. Patients and aneurysm characteristics

A total of 248 patients (155 women [62.5 %] and 93 men [37.5 %]), and 293 intracranial aneurysms were included. Thirty-six patients (14.5 %) had multiple aneurysms. A total of 199 aneurysms (67.9 %) were ruptured aneurysms with subarachnoid hemorrhage, and 94 aneurysms (32.1 %) were unruptured aneurysms. The aneurysm data were randomly divided into training cohorts ($n = 205$) and test cohorts ($n = 88$) in a ratio of 7:3. The comparison results of the clinical data of patients in the ruptured and unruptured groups in the training and test cohorts are shown in Table 1. The training and test cohorts showed statistically significant differences in age and aneurysm location ($P < 0.05$).

Univariate analysis of the ruptured versus the unruptured group found significant statistical differences in age, stroke, and abnormal uric acid levels ($P < 0.05$). Multivariate analysis showed that age, hypertension, stroke, abnormal uric acid, and aneurysm location (anterior cerebral artery [ACA], middle cerebral artery [MCA], anterior communicating artery [ACoA], basilar artery [BA], or internal carotid artery [ICA]) were independent clinical risk factors ($P < 0.05$). Univariate and multivariate analyses are presented in Table 2.

3.2. Radiomics model construction

A total of 1211 features were included in the intra-group correlation coefficient test. 420 features were excluded due to the intraclass correlation coefficient (ICC) < 0.8 . Finally, ten radiomics features were selected after using a variance filter with a threshold of 1.0, ANOVA, and LASSO with 10-fold cross-validation algorithms. The overall consistency of the features among readers was good (average ICC = 0.86, range 0.80–0.92). Moreover, the ten selected features showed a significant difference between the ruptured and unruptured status of aneurysms (Fig. 3A–B). In LASSO, each case’s radiomics score was derived by weighting the ten radiomic features and their coefficients (Fig. 3C–D).

Table 1
Clinical risk factors for aneurysm rupture in the study population.

Variable	Training cohort (n = 205)		P-value	Testing cohort (n = 88)		P-value
	rupture (n = 139)	unrupture (n = 66)		rupture (n = 60)	unrupture (n = 28)	
Age, years (mean ± SD)	58.47 ± 10.26	62.21 ± 10.69	0.017	56.28 ± 11.58	61.61 ± 11.19	0.046
Sex			0.495			0.949
Male	50 (35.97 %)	27 (40.91 %)		24 (40.00 %)	11 (39.29 %)	
Female	89 (64.03 %)	39 (59.09 %)		36 (60.00 %)	17 (60.71 %)	
Smoking	26 (18.71 %)	10 (15.15 %)	0.532	9 (15.00 %)	6 (21.43 %)	0.658
Drinking	24 (17.27 %)	8 (12.12 %)	0.343	4 (6.67 %)	6 (21.43 %)	0.095
Hypertension	100 (71.94 %)	43 (65.15 %)	0.323	37 (61.67 %)	18 (64.29 %)	0.813
Diabetes mellitus	73 (54.68 %)	30 (45.45 %)	0.217	37 (61.67 %)	6 (21.43 %)	<0.001
Heart disease	11 (7.91 %)	7 (10.61 %)	0.525	3 (5.00 %)	1 (3.57 %)	1.000
Thyroid disease	8 (5.76 %)	4 (6.06 %)	1.000	6 (10.00 %)	1 (3.57 %)	0.538
Stroke	2 (1.44 %)	8 (12.12 %)	0.003	2 (3.33 %)	3 (10.71 %)	0.369
Tumor	3 (2.16 %)	1 (1.52 %)	1.000	0 (0.00 %)	0 (0.00 %)	1.000
Aspirin use	2 (1.44 %)	3 (4.55 %)	0.388	1 (1.67 %)	2 (7.14 %)	0.237
Uric acid abnormal	32 (23.02 %)	5 (7.58 %)	0.007	11 (18.33 %)	4 (14.29 %)	0.868
Hyperlipidemia	15 (10.79 %)	9 (13.64 %)	0.554	5 (8.33 %)	4 (14.29 %)	0.631
Family history of intracranial aneurysm	0 (0.00 %)	0 (0.00 %)	1.000	0 (0.00 %)	1 (3.57 %)	0.318
Aneurysm location			0.007			<0.001
ICA	60 (43.17 %)	38 (57.58 %)		18 (30.00 %)	22 (78.57 %)	
ACA	7 (5.04 %)	0 (0.00 %)		7 (11.67 %)	0 (0.00 %)	
MCA	27 (19.42 %)	8 (12.12 %)		6 (10.00 %)	2 (7.14 %)	
PCA	2 (1.44 %)	4 (6.06 %)		1 (1.67 %)	0 (0.00 %)	
ACoA	38 (27.34 %)	10 (15.15 %)		26 (43.33 %)	2 (7.14 %)	
AChA	2 (1.44 %)	4 (6.06 %)		1 (1.67 %)	1 (3.57 %)	
BA	3 (2.16 %)	2 (3.03 %)		1 (1.67 %)	0 (0.00 %)	
VA	0 (0.00 %)	0 (0.00 %)		0 (0.00 %)	1 (3.57 %)	

Abbreviations: ACA, Anterior cerebral artery; ACoA, Anterior communicating artery; AChA, anterior choroidal artery; BA, Basilar artery; ICA, Internal carotid artery; MCA, Middle cerebral artery; PCA, Posterior cerebral artery; VA, Vertebral artery.

Table 2
Clinical risk factors for aneurysm rupture in the study population.

Variable	Ruptured (n = 199)	Unruptured (n = 94)	Univariate analysis (P-value)	Multivariate analysis (P-value)
Age, years	57.81 ± 10.70	62.03 ± 10.79	0.016	0.036
Sex			0.497	NA
Male	74 (37.2 %)	38 (40.4 %)		
Female	125 (62.8 %)	56 (59.6 %)		
Smoking	35	16	0.534	NA
Drinking	28	14	0.344	NA
Hypertension	137	61	0.324	0.022
Diabetes mellitus	113	36	0.218	NA
Heart disease	14	8	0.526	NA
Thyroid disease	14	5	0.931	NA
Stroke	4	11	0.001	0.004
Tumor	3	1	0.757	NA
Aspirin use	3	5	0.178	NA
Uric acid abnormal	43	9	0.006	0.003
Hyperlipidemia	20	13	0.555	NA
Family history of intracranial aneurysm	0	1	NA	NA
Aneurysm location				
ICA	78 (39.2 %)	60 (63.8 %)	0.053	0.009
ACA	14 (7.0 %)	0 (0.0 %)	0.063	<0.001
MCA	33 (16.6 %)	10 (10.6 %)	0.194	0.002
PCA	3 (1.5 %)	4 (4.3 %)	0.066	NA
ACoA	64 (32.2 %)	12 (12.8 %)	0.053	<0.001
AChA	3 (1.5 %)	5 (5.3 %)	0.066	NA
BA	4 (2.0 %)	2 (2.1 %)	0.707	0.034
VA	0 (0.0 %)	1 (1.1 %)	NA	NA

Abbreviations: ACA, Anterior cerebral artery; ACoA, Anterior communicating artery; AChA, anterior choroidal artery; BA, Basilar artery; ICA, Internal carotid artery; MCA, Middle cerebral artery; NA, not available; PCA, Posterior cerebral artery; VA, Vertebral artery.

3.3. Predictive performance of the clinical, rad-score, and combined models

3.3.1. Discrimination ability

The performance of the models is shown in Table 3 and Fig. 4 A-B. For the assessment of small intracranial aneurysm rupture, the combined clinical–radiomics model achieved a discrimination performance with a AUC of 0.87 (95 % CI, 0.8222–0.919) and 0.85 (95 % CI, 0.757–0.947) in the training and the test cohort, respectively. This performance was better than that of the radiomics model with a AUC of 0.79 (95 % CI, 0.727–0.859, DeLong Test p -value <0.01) and 0.75 (95 % CI, 0.645–0.865, DeLong’s test p -value = 0.015) and that of the clinical factor model with a AUC of 0.75 (95 % CI, 0.683–0.818, DeLong’s test p -value <0.01) and 0.74 (95 % CI, 0.625–0.851, DeLong’s test p -value <0.01) in the training and the test cohort, respectively. Furthermore, sensitivity, specificity, accuracy, precision, and rad-score bar charts were used to assess and compare the discrimination ability in the training and test cohorts between the three models.

3.3.2. Model calibration

Calibration curves were presented in Fig. 4 C-D. In the training and validation cohorts, there were no significant differences ($p > 0.05$), indicating that the radiomics, clinical, and combined models were well-fit.

3.3.3. Clinical utility

The decision curve analysis and nomogram were constructed to determine clinical utility. The decision curve analysis curves are shown in Fig. 5 A-B, which indicated that a model combining the rad-score and clinical factors had a higher net benefit and little overlap within a range from 0.1 to 1.0. Finally, the constructed nomogram shows the multivariable logistic regression weights in Fig. 5 C.

4. Discussion

In our study, we developed and validated a classification model based on radiomics and clinical features to discriminate between ruptured and unruptured intracranial small aneurysms. The proposed model enabled the prediction of intracranial small aneurysm rupture status with a AUC of 0.87 and 0.85 in the training and test cohorts, respectively.

To determine the optimal signature for small ruptured aneurysms classification in the radiomics analysis, four first-orders, two shapes, three GLDMS, and one GLSZM features were screened out in our study, consistently with previous studies [21–23]. GLN features describe the uneven gray distribution in the aneurysm area. The difference in texture features in the CTA images is caused by the uneven distribution of the contrast medium in the aneurysm caused by local blood turbulence. Therefore, these texture features can indirectly reflect the local hemodynamic changes of the aneurysm, and the hemodynamic parameters play an important role in the formation, enlargement, rupture, and recurrence of intracranial aneurysms [22]. Moreover, shape features can reflect the diameter and

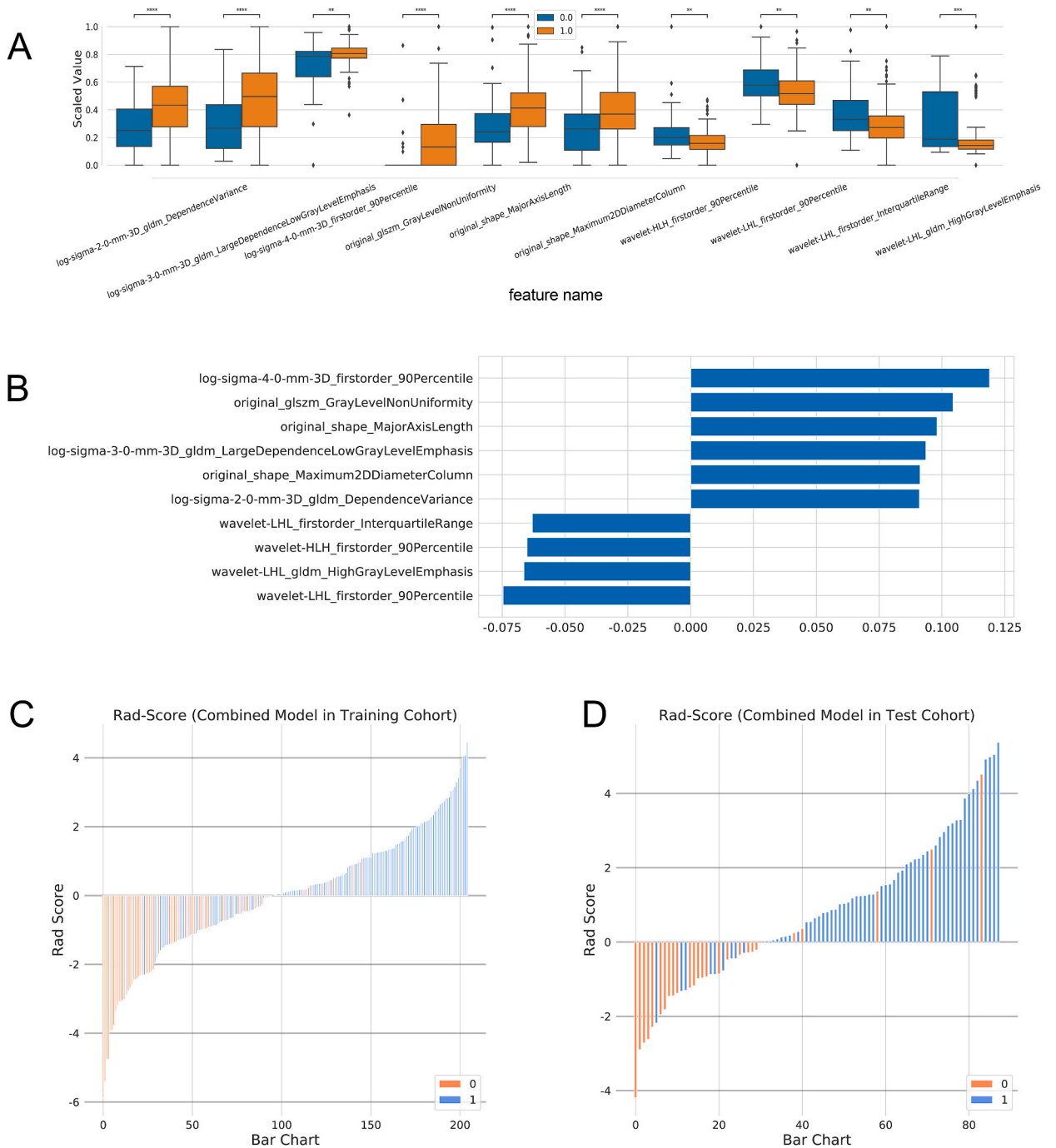


Fig. 3. Radiomics signature score (rad-score) calculation. Top ten features and feature coefficients (feature importance) between the ruptured status of aneurysms (A–B). The radiomics scores (rad-scores) of each patient in the training (C) and test cohorts (D) showed the association of a high rad-score with the risk of aneurysm rupture.

aspect ratio in aneurysm morphology [23]. Although aneurysm morphological parameters are widely used to predict the risk of rupture, there are some deficiencies in their acquisition as the morphological parameters of aneurysms will change with the different projection positions selected by the measurer. However, the computer automatically extracts the radiomics parameters, which significantly reduces human error. Thus, the radiomics features in the aneurysm region based on CTA images can truly and objectively reflect the morphological features of the aneurysm and changes in the hemodynamics within the aneurysm.

We further investigated the predictive model with the clinical factors while adding the clinical factors to the radiomics model for the multivariate logistic analysis. By comparing the C-model, R-model, and CR-model, we found that the CR-model significantly

Table 3
Performance of the clinical, radiomics, and clinical-radiomics models.

Datasets	Models	AUC (95 % CI)	ACC	Precision	SEN	SPE
Training cohorts	C-model	0.75 (0.683–0.818)	0.649	0.807	0.633	0.751
	R-model	0.79 (0.727–0.859)	0.732	0.850	0.734	0.727
	CR-model	0.87 (0.822–0.919)	0.761	0.875	0.755	0.773
Test cohorts	C-model	0.74 (0.625–0.851)	0.705	0.870	0.667	0.786
	R-model	0.75 (0.645–0.865)	0.614	0.825	0.550	0.750
	CR-model	0.85 (0.757–0.947)	0.773	0.917	0.733	0.857

Abbreviations: R-model, radiomics model; C-model, clinical model; CR-model, clinical radiomics model. ACC, accuracy; SEN, sensitivity; SPE, specificity.

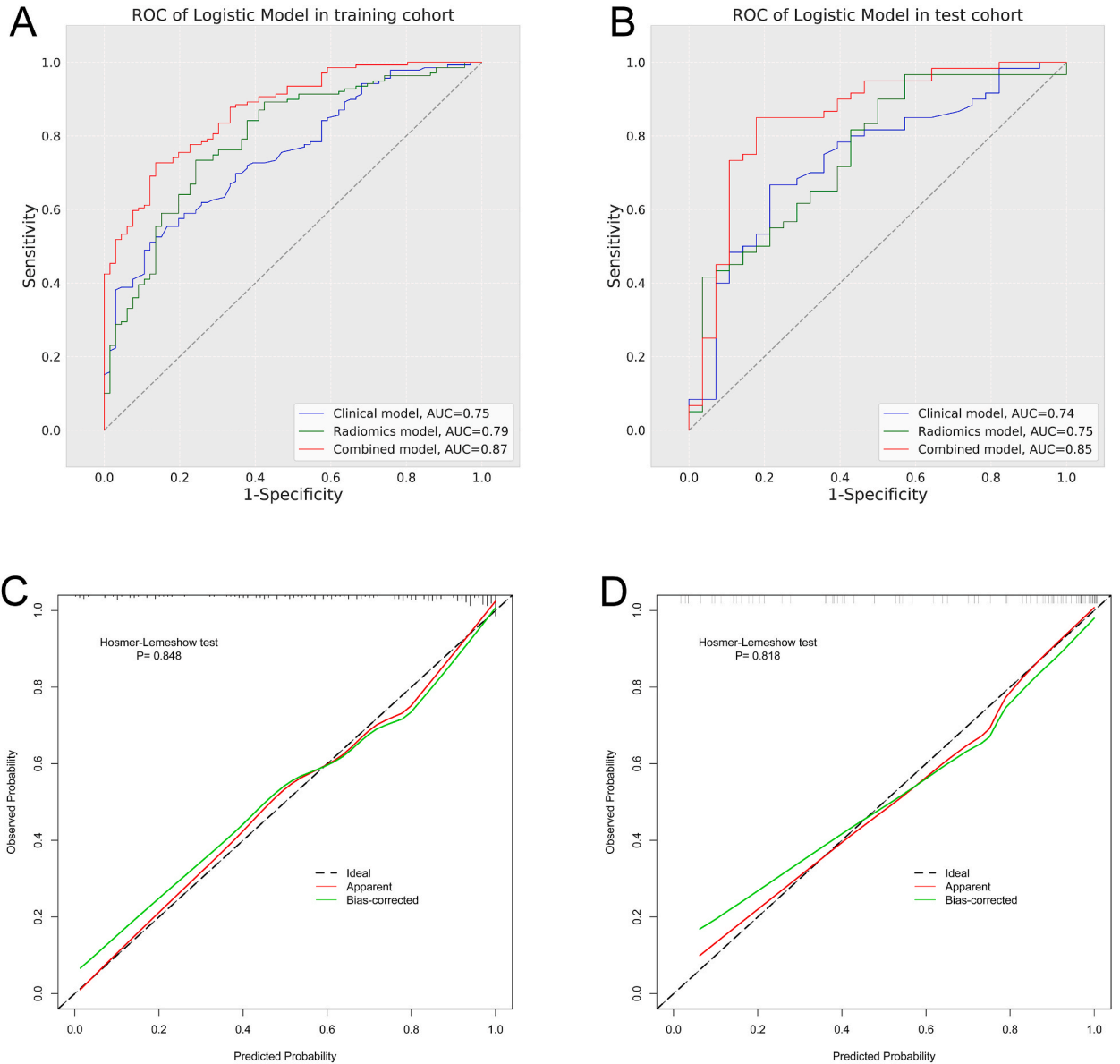


Fig. 4. Receiver operating characteristic (ROC) curves and calibration curve of the radiomics model (R model), clinical model (C model), and clinical radiomics model (CR model). The operating characteristic curves of the three models in the training (A) and test cohorts (B). Calibration curve of the three models in the training (C) and test cohorts (D).

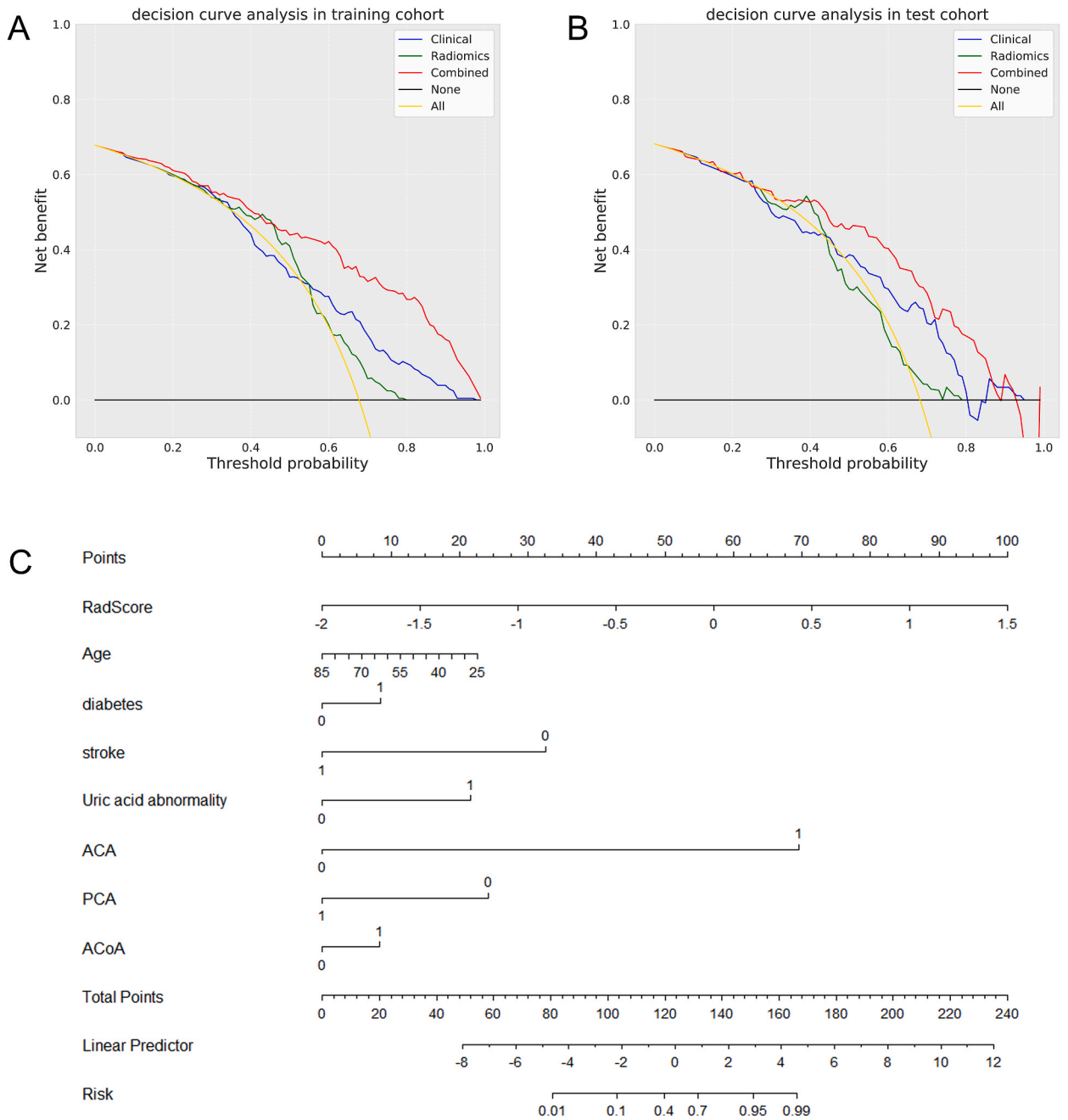


Fig. 5. Decision curve analysis and comprehensive nomogram for small aneurysms in all patients. **(A)** Training and test cohorts **(B)** decision curve analysis of the clinical model, radiomics model, and clinical–radiomics model with the threshold probability on the x-axis and the net benefit on the y-axis. Nomogram for the prediction of small aneurysm ruptures **(C)**.

improved predictive performance. The CR-model had a AUC of 0.87 and 0.85 in the training and the test cohort, respectively, compared to the R-model with a AUC of 0.79 ($p < 0.01$) and 0.75 ($p = 0.015$) and the C-model with a AUC of 0.75 ($p < 0.01$) and 0.74 ($p < 0.01$) in the training and the test cohort, respectively. Various clinical factors and aneurysm morphological parameters have been suggested to be related to rupture, including age, diabetes history, stroke, abnormal uric acid, and location of aneurysms (ACA, ACoA, PCA) in our study, consistently with previous studies [5,12,13,24] While aneurysm rupture risk has been controversially linked to age, age plays an important role in the treatment decision-making [10]. Previous studies have suggested that the blood vessel walls become more fragile and more prone to cause aneurysm rupture with age [7]. But the univariate and multivariate logistic analyses in our study showed that younger patients had a greater risk of aneurysm rupture than older patients, which was consistent with findings from Erdem et al. [25]. This is probably due to the fact that middle-aged patients have a low awareness of or pay little attention to their

cerebrovascular diseases and do not adequately engage in secondary prevention of acute stroke. It is widely accepted that the location of aneurysms affects aneurysm rupture [5]. The origin of the posterior communicating artery, including ACA, MCA, and PCA confer a higher risk of rupture, because the aneurysm near the circle of Willis or the bifurcation of vessels may be related to weak tissue support and local imbalance of blood flow [12]. In our nomogram analysis, aneurysms located in the ACA, ACoA, and PCA were risk factors for intracranial aneurysm rupture, which was consistent with findings from Thompson et al. [10]. However, the location of aneurysms in the MCA was not a risk factor. MCA aneurysms are generally larger in diameter, and only small aneurysms were included in our study.

Zhu et al. [26] conducted a stability study based on clinical and imaging data of intracranial aneurysms and showed that a machine learning model had significant advantages in the stability analysis of intracranial unruptured aneurysms. Thus, they found a AUC of 0.867, specificity of 92.9 %, and an accuracy of 82.4 %. Our work differs from previous studies in two main ways. First, patients with aneurysms (diameter <5 mm) were enrolled to construct the nomogram in our study, which differed from previous studies. Due to the limited ability of CTA to detect small aneurysms, there are relatively few studies on small aneurysms. Second, the CR model established by adding radiomics features to the traditional clinical model can better predict and classify the risk of rupture of intracranial small aneurysms.

There are, however, some limitations to our study. First, the study was a single-center study with a relatively small population, and it was not validated in the external validation cohort. Our next study will involve several centers and a larger number of patients in order to validate our model. Second, this study involved post-aneurysm rupture imaging, which may have been amplified by the accuracy of the radiomics shape features and first-order features extraction. Third, to extract radiomics features from CTA images, manual segmentation was used. The agreement on manual segmentation was validated, but it was a time-consuming process likely to cause small inconsistencies between radiologists. Meanwhile, manual segmentation based on small aneurysms <5 mm may lead to local data bias. To solve the repeatability, reliability, and accuracy problems, an automatic aneurysm segmentation system could be designed. Furthermore, deep learning algorithms [27,28] can further improve the performance of the diagnostic model. Last, the model did not include all aneurysm morphological and hemodynamics parameters [29]. Should these parameters be added to the model, they may improve the accuracy of the model evaluation, but also increase the complexity of the model and limit its application in clinical practice [30].

In conclusion, we evaluated and analyzed the rupture status classification of small intracranial aneurysms through clinical, radiomics, and combined clinical–radiomics models. Combining radiomics models with clinical models can provide additional net benefits for the rupture classification of small intracranial aneurysms and generate a simple and visual rupture risk score nomogram for small aneurysms. These new developments could be helpful in guiding clinical rational intervention in small aneurysms (<5 mm).

Ethics committee

Due to the absence of any individually identifying information in the dataset, local Institutional Review Board (IBR) granted an exemption to informed consent (IRB: 2021-FSK-K009).

CRedit authorship contribution statement

Yu Ye: Writing – review & editing, Writing – original draft, Conceptualization. **Jiao Chen:** Writing – review & editing, Data curation. **Xiaoming Qiu:** Methodology. **Jun Chen:** Methodology. **Xianfang Ming:** Data curation. **Zhen Wang:** Software. **Xin Zhou:** Validation. **Lei Song:** Writing – review & editing, Supervision, Project administration, Conceptualization.

Declaration of competing interest

The authors declare that they have no known competing financial interests or personal relationships that could have appeared to influence the work reported in this paper.

Acknowledgments

We gratefully appreciate Xiaoming Qiu, Xianfang Ming, Zhen Wang for invaluable help in data collection. We thank Lei Song, Xin Zhou for the final revision of the manuscript. We would like to thank Jun Chen for his help with statistical review. We would also like to thank Editage (www.editage.cn) for English language editing. Yu Ye and Jiao Chen were responsible for the study concept and design.

References

- [1] J. Claassen, S. Park, Spontaneous subarachnoid haemorrhage, *Lancet* 400 (10355) (2022) 846–862. [https://doi.org/10.1016/S0140-6736\(22\)00938-2](https://doi.org/10.1016/S0140-6736(22)00938-2).
- [2] H. Jin, J. Geng, Y. Yin, et al., Fully automated intracranial aneurysm detection and segmentation from digital subtraction angiography series using an end-to-end spatiotemporal deep neural network, *J. Neurointerventional Surg.* 12 (10) (2020) 1023–1027. <https://doi.org/10.1136/neurintsurg-2020-015824>.
- [3] N. Varble, V.M. Tutino, J. Yu, et al., Shared and distinct rupture discriminants of small and large intracranial aneurysms, *Stroke* 49 (4) (2018) 856–864. <https://doi.org/10.1161/STROKEAHA.117.0199294>.
- [4] D. Backes, G.J. Rinkel, K.G. Laban, A. Algra, M.D. Vergouwen, Patient- and aneurysm-specific risk factors for intracranial aneurysm growth: a systematic review and meta-analysis, *Stroke* 47 (4) (2016) 951–957. <https://doi.org/10.1161/STROKEAHA.115.0121625>.
- [5] RD Jr Brown, J.P. Broderick, Unruptured intracranial aneurysms: epidemiology, natural history, management options, and familial screening, *Lancet Neurol.* 13 (4) (2014) 393–404. [https://doi.org/10.1016/S1474-4422\(14\)70015-8](https://doi.org/10.1016/S1474-4422(14)70015-8).

- [6] A. Malhotra, X. Wu, H.P. Forman, et al., Growth and rupture risk of small unruptured intracranial aneurysms: a systematic review, *Ann. Intern. Med.* 167 (1) (2017) 26–33. <https://doi.org/10.7326/M17-0246>.
- [7] J.P. Greving, M.J. Wermer, R.D. Brown Jr., et al., Development of the PHASES score for prediction of risk of rupture of intracranial aneurysms: a pooled analysis of six prospective cohort studies, *Lancet Neurol.* 13 (1) (2014) 59–66. [https://doi.org/10.1016/S1474-4422\(13\)70263-1](https://doi.org/10.1016/S1474-4422(13)70263-1).
- [8] H.P. Lai, K.M. Cheng, S.C. Yu, et al., Size, location, and multiplicity of ruptured intracranial aneurysms in the Hong Kong Chinese population with subarachnoid haemorrhage, *Hong Kong Med. J.* 15 (4) (2009) 262–266.
- [9] P. Dolati, D. Pittman, W.F. Morrish, J. Wong, G.R. Sutherland, The frequency of subarachnoid hemorrhage from very small cerebral aneurysms (< 5 mm): a population-based study, *Cureus* 7 (6) (2015) e279. <https://doi.org/10.7759/cureus.279>.
- [10] B.G. Thompson, R.D. Brown, S. Amin-Hanjani, et al., Guidelines for the management of patients with unruptured intracranial aneurysms: a guideline for healthcare professionals from the American heart association/American stroke association, *Stroke* 46 (8) (2015) 2368–2400. <https://doi.org/10.1161/STR.000000000000070>.
- [11] A. Can, V.M. Castro, Y.H. Ozdemir, et al., Alcohol consumption and aneurysmal subarachnoid hemorrhage, *Transl Stroke Res* 9 (1) (2018) 13–19. <https://doi.org/10.1007/s12975-017-0557-z>.
- [12] K. Suzuki, M. Izumi, T. Sakamoto, M. Hayashi, Blood pressure and total cholesterol level are critical risks especially for hemorrhagic stroke in Akita, Japan, *Cerebrovasc. Dis.* 31 (1) (2011) 100–106. <https://doi.org/10.1159/000321506>.
- [13] A.E. Lindgren, M.I. Kurki, A. Riihinen, et al., Type 2 diabetes and risk of rupture of saccular intracranial aneurysm in eastern Finland, *Diabetes Care* 36 (7) (2013) 2020–2026. <https://doi.org/10.2337/dc12-1048>.
- [14] D. Kashiwazaki, S. Kuroda, Sapporo SAH Study Group, Size ratio can highly predict rupture risk in intracranial small (<5 mm) aneurysms, *Stroke* 44 (8) (2013) 2169–2173. <https://doi.org/10.1161/STROKEAHA.113.001138>.
- [15] Z. Duan, Y. Li, S. Guan, et al., Morphological parameters and anatomical locations associated with rupture status of small intracranial aneurysms, *Sci. Rep.* 8 (1) (2018) 6440. <https://doi.org/10.1038/s41598-018-24732-1>.
- [16] P. Jiang, Q. Liu, J. Wu, et al., A novel scoring system for rupture risk stratification of intracranial aneurysms: a hemodynamic and morphological study, *Front. Neurosci.* 12 (2018) 596. <https://doi.org/10.3389/fnins.2018.00596>.
- [17] A. Zwanenburg, M. Vallières, M.A. Abdalah, et al., The image biomarker standardization initiative: standardized quantitative radiomics for high-throughput image-based phenotyping, *Radiology* 295 (2) (2020) 328–338. <https://doi.org/10.1148/radiol.2020191145>.
- [18] O. Alwalid, X. Long, M. Xie, et al., CT angiography-based radiomics for classification of intracranial aneurysm rupture, *Front. Neurol.* 12 (2021) 619864. <https://doi.org/10.3389/fneur.2021.619864>.
- [19] Y. Zhang, C. Ma, S. Liang, et al., Morphologic feature elongation can predict occlusion status following pipeline embolization of intracranial aneurysms, *World Neurosurg* 119 (2018) e934–e940. <https://doi.org/10.1016/j.wneu.2018.08.007>.
- [20] J. Liu, Y. Chen, L. Lan, et al., Prediction of rupture risk in anterior communicating artery aneurysms with a feed-forward artificial neural network, *Eur. Radiol.* 28 (8) (2018) 3268–3275. <https://doi.org/10.1007/s00330-017-5300-3>.
- [21] S. Tanioka, F. Ishida, A. Yamamoto, et al., Machine learning classification of cerebral aneurysm rupture status with morphologic variables and hemodynamic parameters, *Radiol Artif Intell.* 2 (1) (2020) e190077. <https://doi.org/10.1148/ryai.2019190077>.
- [22] C. Ou, W. Chong, C.Z. Duan, X. Zhang, M. Morgan, Y. Qian, A preliminary investigation of radiomics differences between ruptured and unruptured intracranial aneurysms, *Eur. Radiol.* 31 (5) (2021) 2716–2725. <https://doi.org/10.1007/s00330-020-07325-3>.
- [23] Q. Liu, P. Jiang, Y. Jiang, et al., Prediction of aneurysm stability using a machine learning model based on PyRadiomics-derived morphological features, *Stroke* 50 (9) (2019) 2314–2321. <https://doi.org/10.1161/STROKEAHA.119.025777>.
- [24] S. Juvela, M. Korja, Intracranial aneurysm parameters for predicting a future subarachnoid hemorrhage: a long-term follow-up study, *Neurosurgery* 81 (3) (2017) 432–440. <https://doi.org/10.1093/neuros/nyw049>.
- [25] E. Güresir, H. Vatter, P. Schuss, et al., Natural history of small unruptured anterior circulation aneurysms: a prospective cohort study, *Stroke* 44 (11) (2013) 3027–3031. <https://doi.org/10.1161/STROKEAHA.113.001107>.
- [26] W. Zhu, W. Li, Z. Tian, et al., Stability assessment of intracranial aneurysms using machine learning based on clinical and morphological features, *Transl Stroke Res* 11 (6) (2020) 1287–1295. <https://doi.org/10.1007/s12975-020-00811-2>.
- [27] Z. Shi, G.Z. Chen, L. Mao, et al., Machine learning-based prediction of small intracranial aneurysm rupture status using CTA-derived hemodynamics: A multicenter study, *AJNR Am J Neuroradiol* 42 (4) (2021) 648–654. <https://doi.org/10.3174/ajnr.A7034>.
- [28] A. Park, C. Chute, P. Rajpurkar, et al., Deep learning-assisted diagnosis of cerebral aneurysms using the HeadXNet model, *JAMA Netw. Open* 2 (6) (2019) e195600. <https://doi.org/10.1001/jamanetworkopen.2019.5600>.
- [29] H. Rajabzadeh-Oghaz, J. Wang, N. Varble, et al., Novel models for identification of the ruptured aneurysm in patients with subarachnoid hemorrhage with multiple aneurysms, *AJNR Am J Neuroradiol* 40 (11) (2019) 1939–1946. <https://doi.org/10.3174/ajnr.A6259>.
- [30] N. Etmann, G.J. Rinkel, Unruptured intracranial aneurysms: development, rupture and preventive management, *Nat. Rev. Neurol.* 12 (12) (2016) 699–713. <https://doi.org/10.1038/nrneurol.2016.150>.